Journal of Magnetism and Magnetic Materials 549 (2022) 168983

Contents lists available at ScienceDirect

Journal of Magnetism and Magnetic Materials

journal homepage: www.elsevier.com/locate/jmmm

Research articles

Experimental characterization of the effect of uniaxial stress on magnetization and iron losses of electrical steel sheets cut by punching process

I.T. Gürbüz [a,*], F. Martin [a], U. Aydin [b], A.B. Asaf Ali [c], M. Chamosa [d], P. Rasilo [e], A. Belahcen [a]

[a] Department of Electrical Engineering and Automation, Aalto University, FI-00076 Espoo, Finland
[b] ABB Oy, Marine and Ports, FI-00232 Helsinki, Finland
[c] ABB Switzerland Ltd, Process Industries, CH-5405, Baden, Switzerland
[d] ABB SA, ES-48510, Trapagarán (Vizcaya), Spain
[e] Unit of Electrical Engineering, Tampere University, FI-33720 Tampere, Finland

ARTICLE INFO

Keywords:
Cutting
Electrical steel
Iron losses
Punching
Uniaxial stress

ABSTRACT

The effect of uniaxial stress on iron losses of M400-50A grade non-oriented electrical steel sheets cut by punching process is experimentally studied. Samples cut along the rolling and transverse directions and having different number of cutting edges are used for this purpose. Measurements are carried out in the range of 10–100 Hz frequency of sinusoidal excitations at different magnetization levels under varying uniaxial stress by using a single sheet tester. The iron losses are obtained from the measurements and comparative analyses are made for different cases. The study shows that the effect of stress on the iron losses of the punched samples varies depending on the degradation level that the samples have after the cutting process. By considering this varying effect, when the combined effect of stress and punching is analyzed, it is observed that the iron losses increased up to 55.2% under compressive stress. It is also observed that the increase in the losses due to the effect of cutting can be recovered by applying tensile stress.

1. Introduction

Electrical steel sheets are usually cut to specific shapes by different techniques during the manufacturing process for appropriate usage in electrical machine parts. These processes cause degradation in the magnetic properties of the electrical steel sheets and increase the iron losses [1–3]. In addition to the residual stress introduced by manufacturing processes, materials are also subjected to additional mechanical stress due to the operating conditions of the machines [4–6]. Due to these mechanical stresses, the magnetic properties and the iron losses of the materials are further affected. In order to model and analyze the electrical machines more accurately, it is needed to investigate the combined effect of stress and cutting on magnetization and iron losses of the electrical steel sheets.

Effect of different cutting techniques on magnetization and iron losses of electrical sheets were studied in several studies experimentally. In these studies, waterjet cutting [7–9], electrical discharge machining (EDM) [10–12], laser-cutting [9,12–17], and different mechanical cutting techniques such as guillotine [1,10,15,16] and punching [2,3,17–20] were studied. Among these cutting techniques, EDM can only cut one sheet at a time by following the line cut; whereas, the laser and waterjet cutting follow a similar process with the possibility to cut multiple sheets. Alternatively, punching can cut a whole surface at once for a single sheet pressed between dies. Hence, punching presents a faster cutting rate for the electrical steel sheets used in electrical machines.

Several comparative analyses for these cutting techniques were conducted. Waterjet cutting was compared with mechanical cutting in [7,8] and laser-cutting in addition to mechanical cutting in [9]. Similarly, EDM was compared with laser cutting in [11,12] and mechanical cutting in [10], and laser-cutting was compared with mechanical cutting in [15–17]. The studies related to the effect of cutting are in agreement with the result that the cutting deteriorates the magnetization and increases the iron losses. Nevertheless, the comparative analyses in [7–12,15–17] show that the amount of the deterioration and the increase in the losses varies depending on the cutting technique. It was found that mechanical and laser-cutting techniques affect the magnetization and iron losses more than waterjet cutting [7–9] and EDM [10,11]; however, the superiority of mechanical and laser-cutting techniques among each other is still controversial. So far, the selected literature

* Corresponding author.
E-mail address: ismet.t.gurbuz@aalto.fi (I.T. Gürbüz).

https://doi.org/10.1016/j.jmmm.2021.168983
Received 2 June 2021; Received in revised form 12 November 2021; Accepted 22 December 2021
Available online 8 January 2022

studies in [1–3,7–20] showed and analyzed the effect of cutting for different techniques extensively. However, all these studies focused solely on the effect of cutting on the magnetization or iron losses, and the effect of additional stress on the cut samples was not considered separately.

The effect of mechanical stress on the magnetic properties and iron losses of the materials was also widely studied. Experimental studies were performed for uniaxial [21–30], biaxial [31,32], and multiaxial [33–36] cases. In these studies, the effect of compression [21,22], tension [23–25], and both tension and compression [26–36] were investigated. While in [25,26,32,33] the effect of stress solely on the magnetic properties was studied, in [21–24,27–29,31,35,36] the effect of stress on the iron losses was studied additionally.

The outcomes of these studies demonstrate that compressive stress deteriorates the magnetization and increases the iron losses along the applied direction. On the other hand, low tensile stress improves the magnetization and reduces the iron losses, while high tensile stress shows similar effect to the compressive stress along the applied direction. It was reported in [22,23,30] that the effect of stress on the magnetization and iron losses exhibits quantitative differences for the rolling direction (RD) and transverse direction (TD), which can be attributed to anisotropic behavior of the material as a result of its crystallographic texture [37]. All these selected literature studies in [21–36] present highly relevant results showing how the stress affects the electrical steel sheets. Nonetheless, in none of these studies, the degradation caused by cutting was not addressed properly, and the effect of stress on the cut samples was not quantified based on the different deterioration levels caused by cutting.

The literature study shows that even though the effect of stress and cutting were studied separately in several studies comprehensively, their combined effect on the magnetization and iron losses has not been addressed properly. Different local regions of the materials used in electrical machine parts are exposed to variant levels of degradation due to cutting. In order to model and simulate the electrical machines parts subjected to additional stress more accurately, it is needed to consider the effect of stress and cutting together. Therefore, in this article, the effect of stress on the magnetic properties and iron losses of the punched non-oriented electrical steel sheets used in conventional electrical machines are experimentally determined for the first time. The remainder of this paper is organized as follows. In Section 2, the measurement system is described in detail. The measurement results and the analyses based on those results are presented in Section 3. Then, Section 4 summarizes the most important findings of this study.

2. Measurement system

2.1. Preparation of samples

Measurements were performed on M400-50 A grade non-oriented electrical steel sheets, which are cut by EDM and punching to 24, 12, 8, and 6 mm wide strips with a length of 280 mm. For the measurements, 24 mm wide samples were then assembled from 1 × 24 mm, 2 × 12 mm, 3 × 8 mm, and 4 × 6 mm strips. Fig. 1 shows the geometry of the assembled samples, which consist of two sets in terms of the cutting direction. The first set includes the samples cut along the RD and the second set includes the samples cut along the TD.

Based on the experiments performed in the literature, it was found that EDM-cutting causes little degradation in the materials compared to the punching [10,11]. In order to see the effect of punching on the magnetization and iron losses of the materials, the EDM-cut sample is taken as a reference for the comparisons. The details of the assembled samples are given in Table 1.

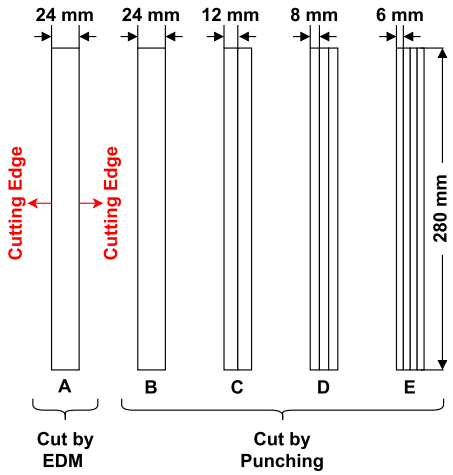

Fig. 1. Assembled samples for the measurements. The height of the samples is 280 mm, and the total width of the samples is 24 mm. The samples are assembled by joining different numbers of strips.

Table 1
The details of the assembled samples. Sample A is EDM-cut and taken as a reference for comparisons with the other samples.

Sample	No. of Strips	Cutting Type
A	1	EDM
B	1	Punching
C	2	Punching
D	3	Punching
E	4	Punching

2.2. Measurement procedure

The measurements were performed by using a self-made modified single sheet tester (SST), a NI USB-6251-based data acquisition device (DAQ) connected to a PC with a MATLAB-based waveform control and an Elgar SW5250 A power supply. In Fig. 2, the SST and positioning of the sample and search coils are shown.

The SST consists of a magnetizing core, a stressing mechanism, and a single sheet sample. The sample is aligned with the stressing mechanism by clamping the sample ends with metallic plates. In addition, to avoid buckling of the sample under compressive loading, the sample is supported from the top and bottom by glass fiber retention plates. In order to measure the magnetic flux density $B(t)$ and magnetic field strength $H(t)$, a B-coil with 10 turns and a H-coil with 400 turns are placed in the middle of the sample. The B-coil surrounds the surface of the sample, and the H-coil is located on the top of the sample. The dimensions of the H-coil are 24 mm × 24 mm × 0.5 mm; therefore, the cross-sectional area is 24 mm × 0.5 mm, and thus the H-coil covers the entire width of the samples. Stress is applied to the samples with a screw mechanism through a spring for a better control of stress resolution. The stress value is read from a load cell. In this study, we are interested in the average quantities of the magnetic flux density and the magnetic field strength. Therefore, the local distribution of the quantities in the damaged and undamaged zones was not studied separately.

In Fig. 3, a diagram showing the measurement procedure is given. Initially, the PC sends a command to the DAQ, and the DAQ sends a control signal $U_c(t)$ to the AC power supply. This reference signal is amplified with the gain of the power supply K_s such that

$$U_s(t) = K_s U_c(t). \tag{1}$$

After the amplification, the power supply sends the supply voltage $U_s(t)$ to the magnetizing coil of the SST. The incoming primary $U_s(t)$ voltage

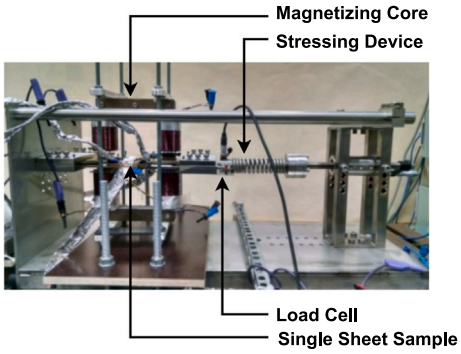

(a)

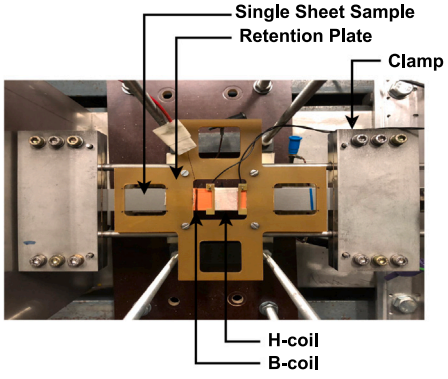

(b)

Fig. 2. Single sheet tester (a) and positioning of a single sheet sample and search coils (b).

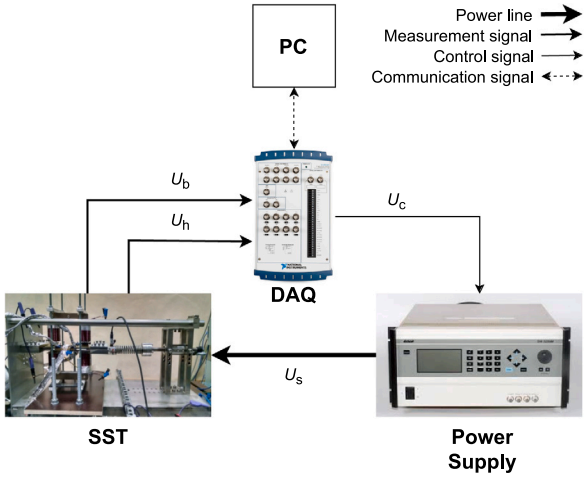

Fig. 3. Schematic diagram of the measurement procedure.

creates a varying flux in the sample, and the flux induces voltages in the B-coil and H-coil. Then, the signals from the B-coil $U_b(t)$ and H-coil $U_h(t)$ are transmitted to the PC through the DAQ. In the PC, the flux density $B(t)$ and the field strength $H(t)$ are calculated by using the relationship in Faraday's law as given by Eq. (2) and (3).

$$B(t) = \frac{1}{N_b A_b} \int_0^T U_b(t)dt \tag{2}$$

$$H(t) = \frac{1}{N_h A_h \mu_0} \int_0^T U_h(t)dt \tag{3}$$

where N_b and N_h are the number of turns in the B-coil and H-coil, and A_b and A_h are the cross-sectional areas of the coils. After obtaining $B(t)$ and $H(t)$, according to the control mechanism in the PC, a new control signal is sent to the power supply and the same procedure continues as long as the control mechanism continues. The purpose of the control mechanism is to force $B(t)$ to be sinusoidal. When it is obtained, the control mechanism ends and the measurement results are recorded.

2.3. Control mechanism

Initially, a sinusoidal voltage is sent to the SST. Due to the non-linearity of the sample, the induced voltages in the B-coil become non-sinusoidal above the saturation level. In order to control the waveform to be sinusoidal, amplitude and waveform controls are applied.

In amplitude control, ratio ϵ^i_{amp} between the amplitude of the measured flux density B^i and reference flux density B_{ref} at iteration i is found, and the new control signal U_c^{i+1} is sent by dividing the control signal at the previous iteration U_c^i with the obtained ratio ϵ^i_{amp} such that

$$\epsilon^i_{amp} = \frac{\max(B^i)}{\max(B_{ref})} \tag{4}$$

$$U_c^{i+1} = \frac{U_c^i}{\epsilon^i_{amp}}. \tag{5}$$

The iterative process continues until ϵ^i_{amp} is below the pre-set tolerance.

The waveform control is based on the adaptive feedback control principle presented in [38]. The new control signal U_c^{i+1} is obtained by including the proportional K_P and K_I terms such that

$$U_c^{i+1} = U_c^i + K_P \frac{U^i_{c1}}{U^i_{b1}}(U^i_b - U_{b,ref}) + K_I \frac{U^i_{c1}}{B^i_1}(B^i - B_{ref}) \tag{6}$$

where U^i_{c1}, U^i_{b1} and B^i_1 are the fundamental components of the control signal U^i_c, B-coil voltage U^i_b, and B^i, respectively. $U_{b,ref}$ stands for the reference of the B-coil voltage.

Initially, the amplitude control is performed. After adjusting the amplitude properly, the waveform control begins and continues until the convergence criterion is met. The convergence criterion is checked at each iteration based on a relative error calculation. The relative error ϵ^i_{wav} is calculated by

$$\epsilon^i_{wav} = \frac{\left\| B^i - B^i_{ref} \right\|}{\left\| B_{ref} \right\|}. \tag{7}$$

The convergence criterion is met when $\epsilon^i_{wav} < 1\%$. The control mechanism is shown in Fig. 4 as a flow chart.

2.4. Performed measurements

Our objective is to study the effect of uniaxial stress on magnetization and iron losses of the punched non-oriented electrical sheets used in conventional electrical machines, for which the fundamental frequency is 50–100 Hz. For this purpose, measurements were performed for varying frequency and stress values at several magnetization levels in the range of 0.63 T - 1.5 T. Details of the measurement variables are given in Table 2. It should be noted that the negative values of the stress correspond to compression; whereas, the positive values correspond to tension. Although the measurements were made under different magnetization levels, the results are presented for 1.5 T magnetization level, which is the standard level for characterizing steel sheets [39]. The findings are similar for the other magnetization levels in terms of the analyses presented for 1.5 T magnetization level.

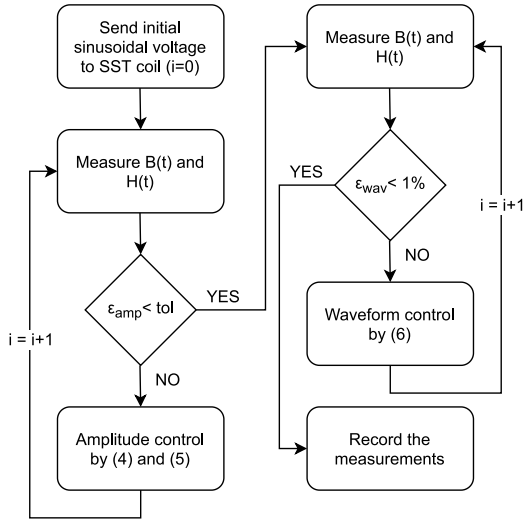

Fig. 4. Flow chart of the control mechanism for the flux density waveform.

Table 2
Flux density, frequency, and stress values of the performed measurements.

Flux density	0.63, 0.83, 1.04, 1.25, 1.5 T
Frequency	10, 20, 50, 100 Hz
Stress	−30, −20, −10, 0, 10, 20, 30, 40, 60, 80 MPa

3. Results and discussion

3.1. Measurement results

The measurements for the cases shown in Table 2 were performed and B–H curves were obtained for each case. In this section, example B–H curves that show the effect of the punching and stress will be given at 10 Hz for the purpose of demonstration.

In Fig. 5, B–H curves for the stress-free case of the least degraded sample (sample A) and the most degraded sample (sample E) at 10 Hz frequency are given. It is seen that as the degradation on the material due to cutting increases, the average permeability of the material reduces. In Fig. 6, B–H curves of sample A under different stress values at 10 Hz frequency are given. When the low tensile stress of 20 MPa is applied, the average permeability of the material improves; whereas, the application of high tensile stress of 80 MPa reduces the average permeability. Additionally, the application of compressive stress of −30 MPa reduces the average permeability and increases the coercive field significantly.

The characteristics of the B–H curves for the samples cut along the RD and TD in Fig. 5 show that at stress-free case, the material is not isotropic as assumed in the simulation of electrical machines. This anisotropy is attributed to the crystallographic texture of the material [37]. Considering the B–H curves in Fig. 6, it is seen that the effect of stress on the average permeability also varies for the samples cut along the RD and TD depending on the applied stress level. For instance, at 20 MPa, the average permeability of the sample cut along the RD is almost same as its stress-free case, while the average permeability of the sample cut along the TD improves compared to the its stress-free case. On the other hand, at 80 MPa, the average permeability of the sample cut along the RD reduces compared to its stress free case, while the average permeability of the sample cut along the TD is almost same as its stress-free case. Under −30 MPa, the average permeability reduces for both directions; however, the quantity of decrease is distinctive. Similar results emphasizing the differences

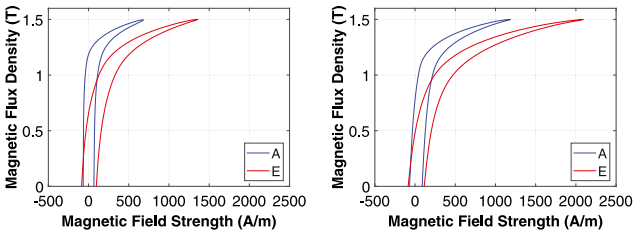

Fig. 5. Measured B–H curves of the samples A and E, cut along the (a) RD and (b) TD, at the stress-free case at 10 Hz.

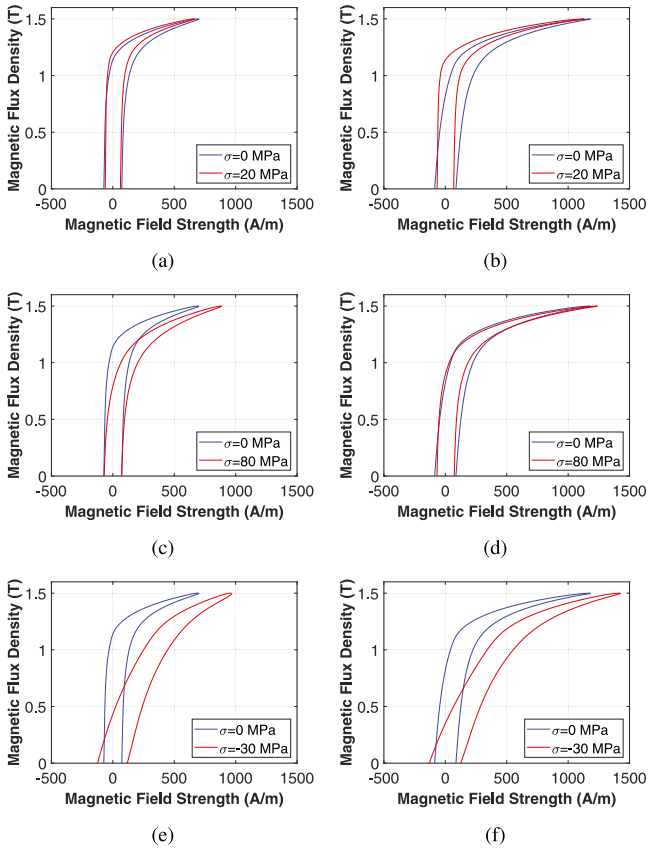

Fig. 6. Measured B–H curves of the sample A at 10 Hz under (a) 20 MPa (c) 80 MPa, (e) −30 MPa for the RD, and under (b) 20 MPa (d) 80 MPa, (e) −30 MPa for the TD.

for the effect of stress on the magnetic properties along the RD and TD were reported in [22,23,30] for different grade non-oriented electrical steel sheets.

Similar to the B–H curves presented in Figs. 5 and 6, the B–H curves of the measurements for each case were obtained. Afterwards, the iron losses were calculated from the B–H curves. The average power loss densities p per supply period T were obtained by

$$p = \frac{1}{T}\int_0^T H(t)\cdot\frac{dB(t)}{dt}dt. \tag{8}$$

3.2. Repeatability of the measurements

The repeatability of the measurements was tested at 1.5 T induction level and 10 Hz and 100 Hz frequencies under different stress levels. Measurements for sample C were repeated 5 times for every case. Before each repetition, the sample was dismantled from the setup. The

search coils of the samples were removed and located again. Then, the sample was assembled back into the SST. Losses for each repetition were calculated, and coefficient of variation, the ratio of the standard deviation to the mean, was found four each case. Fig. 7 shows the coefficient of variation for the measured cases. In the worst case, coefficient of variation was found as 4.15%.

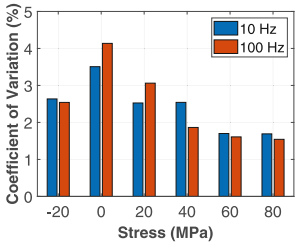

Fig. 7. Coefficient of variation vs stress at 10 Hz and 100 Hz frequencies.

The factors affecting the repeatability are positioning of the B-coil and H-coil on the samples, alignment of the magnetizing cores with respect to the samples, alignment of the stressing mechanisms with respect to the sample, control of the signals, and the change in the temperature of the samples. The effect of these factors was not quantified separately. Similar factors are reported in [40].

3.3. Iron losses

The calculated iron losses of the assembled samples under varying stress levels at 1.5 T induction level and different frequencies are given in Figs. 8 and 9 for the samples cut along the RD and TD, respectively. The iron losses are shown in the y-axis and the applied stress values are shown in the x-axis. In each graph, there are 5 curves illustrating the iron losses of each assembled sample under varying stress values. Based on the previous literature studies in [10,11] and the measurement results presented in Figs. 8 and 9, we considered that the EDM-cutting technology induces very small degradation compared to the punching. Hence, we assumed the number of cutting edges for the EDM-cut sample (sample A) as 0 for the purposes of comparison and demonstration. The number of cutting edges for samples B, C, D, and E corresponds to 2, 4, 6, and 8, respectively.

Figs. 8 and 9 show that the losses increase as the number of cutting edges increases as a result of the degradation introduced by punching process. The application of compressive stress increases the losses further in all samples. On the other hand, the application of tensile stress on the samples with lower number of cutting edges (samples A, B, and C) decreases the losses until different magnitudes of the stress. Beyond these magnitudes, the losses increase again. However, it is observed that the application of tensile stress on the samples with higher number of cutting edges (samples D and E) decreases the losses continuously for the stress range that could be applied with our setup. The difference in the trends shows that the effect of stress on the iron losses of the punched samples changes according to the degradation level that the sample has after the cutting process. In the next section, this effect will be explained in detail.

3.4. Effect of stress on the iron losses of the punched samples

In order to study the effect of stress on the iron losses of the punched samples having an increasing number of cutting edges, the loss values of each sample for different stress levels are normalized to the loss value of the stress-free case of each one separately. The percentage variation of the losses Δp compared to the reference of each sample is calculated by

$$\Delta p = \frac{p(\sigma) - p(0)}{p(0)} \tag{9}$$

where $p(\sigma)$ and $p(0)$ are the iron loss density of the sample for the corresponding stress level and iron loss density of the sample at its

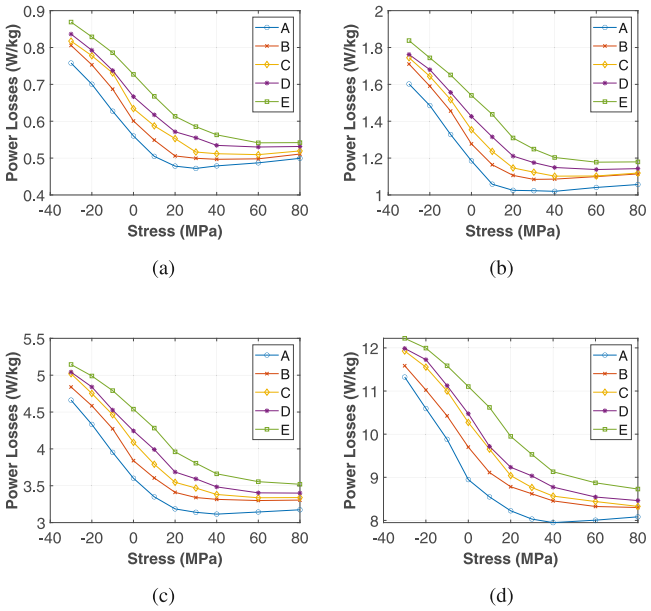

Fig. 8. Iron losses vs stress graphs (a) at 10 Hz, (b) at 20 Hz, (c) at 50 Hz, and (d) at 100 Hz for the samples cut along the RD.

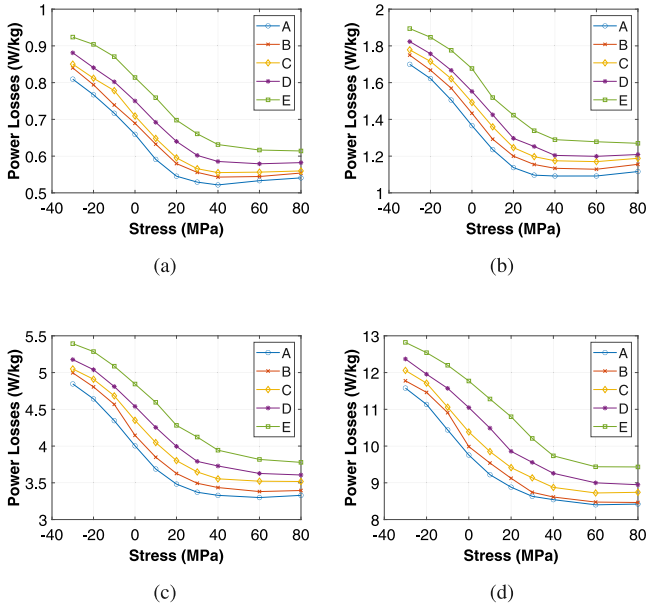

Fig. 9. Iron losses vs stress graphs (a) at 10 Hz, (b) at 20 Hz, (c) at 50 Hz, and (d) at 100 Hz for the samples cut along the TD.

stress-free case (Figs. 8–9). The calculated percentage variations are given in Figs. 10 and 11 at 1.5 T induction level and different frequencies for the samples cut along the RD and TD, respectively. The x-axis and y-axis show the applied stress values and the number of cutting edges that each sample has, respectively. As the measurement results are at discrete values, a linear variation was assumed between the measurement points for visualization purposes. The different colors indicate the percentage variation values of the losses, and the iso-value lines connect the regions having the same percentage variation values. It should be noted that at 0 MPa value, the line is vertical as own reference points of each sample is taken at 0 MPa; therefore, the value of the percentage variation is 0.

According to Figs. 10 and 11, under compressive stress, the loss of each sample increases as the applied stress value increases. When

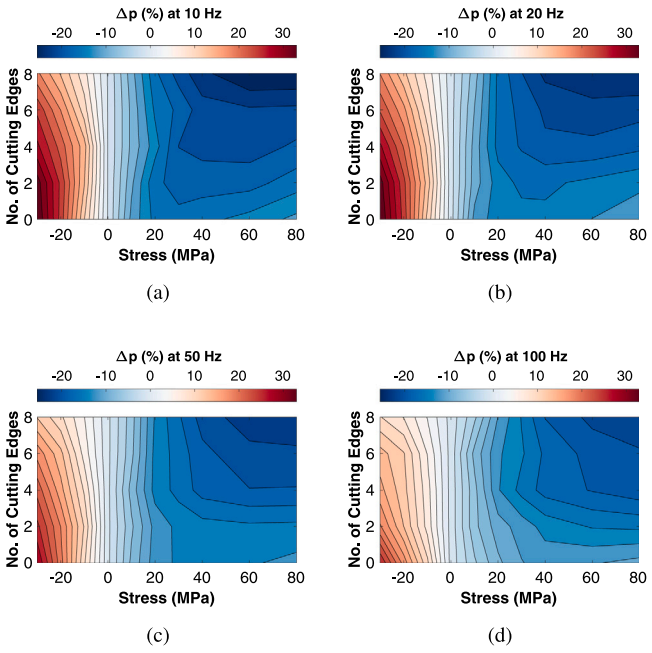

Fig. 10. Percentage variation of the losses (a) at 10 Hz, (b) at 20 Hz, (c) at 50 Hz, and (d) at 100 Hz compared to stress-free case of each sample, which is cut along the RD, separately.

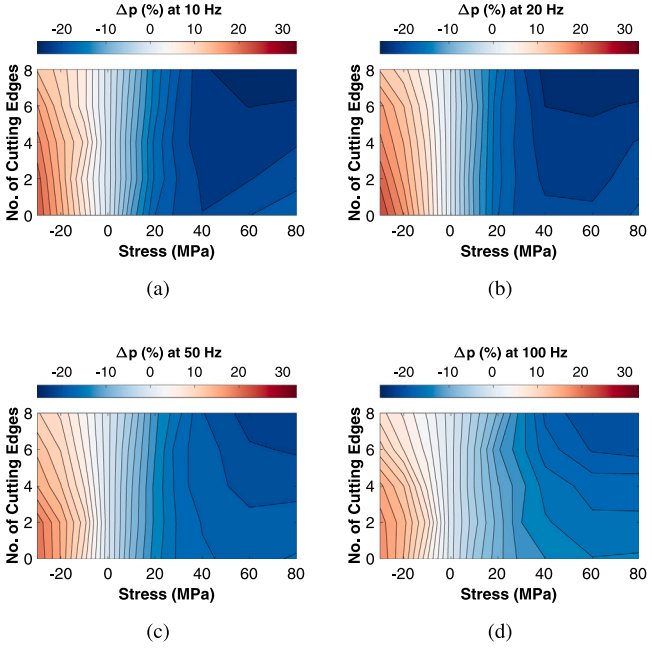

Fig. 11. Percentage variation of the losses (a) at 10 Hz, (b) at 20 Hz, (c) at 50 Hz, and (d) at 100 Hz compared to stress-free case of each sample, which is cut along the TD, separately.

the same value of compressive stress is applied to the samples, the percentage variation of the losses decreases as the number of cutting edges increases. For instance, at 10 Hz and −30 MPa stress level, as the number of cutting edges increases from 0 (sample A) to 8 (sample E), the percentage variation decreases from 35.3% to 19.5% and 22.8% to 13.5% for the samples cut along the RD and TD, respectively. One reason is that when the compressive stress is applied to the already deteriorated sample, the additional deterioration that can be added by compressive stress is limited. As the initial deterioration introduced by the cutting process increases, the deterioration added by the compressive stress decreases.

Under tensile stress, the losses of each sample initially decrease until different threshold values of the applied stress. These thresholds correspond to the states where most of the domains of the material are aligned in the direction of magnetization. Application of additional stress beyond these thresholds increases the losses due to the Villari reversal. As the number of cutting edges increases, the samples become more deteriorated, and more tensile stress is required to align the domains in the direction of magnetization. Therefore, the threshold values become higher as the number of cutting edges increases. At 10 Hz for sample A cut along the RD, the highest percentage variation in the losses is in 20–40 MPa region, where the threshold value is reached. At higher values of stress (40–80 MPa), the percentage variation in the losses decreases due to the increase in the losses. On the other hand, for the samples with the higher number of cutting edges, the regions where the highest percentage variations are observed shift to the higher values of the applied stress, as a result of the higher threshold values. It is observed that sample E has not reached its threshold value even at 80 MPa as the decreasing trend in the losses continues as can be also seen in Figs. 8 and 9. Therefore, at high values of tensile stress, the percentage variations of the losses compared to the stress-free states are more for the samples having higher number of cutting edges. For instance, at 80 MPa, the percentage variation of the losses for sample A cut along the RD is 10.8%; whereas, the percentage variation of the losses for sample E cut along the RD is 25.8%.

It is observed that the percentage variation decreases as the frequency increases. In order to justify the reason behind it, an example loss separation for hysteresis and eddy-current losses was made for the stress-free case by using Jordan's method, which can be expressed as

$$p_{\text{tot}} = k_{\text{hy}} B^2 f + k_{\text{e}} B^2 f^2 \tag{10}$$

where p_{tot} is the total power loss density averaged for RD and TD, and k_{hy} and k_{e} are the hysteresis and eddy-current loss coefficients. The coefficients k_{hy} and k_{e} were obtained by least-squares fitting for each sample separately. While fitting the parameters, data from all measured frequencies and magnetization levels were used. The fitted coefficients for samples A and E are given in Table 3. Based on the fitted parameters, the contribution of the hysteresis and eddy-current losses to the total iron losses was calculated for each frequency. Fig. 12 shows the contribution of losses for (a) sample A and (b) sample E at 1.5 T magnetization level.

Table 3
Fitted loss coefficients for sample A and sample E.

Sample	k_{hy} (W kg^{-1} Hz^{-1} T^{-2})	k_{e} (W kg^{-1} Hz^{-2} T^{-2})
A	0.0258	1.59×10^{-4}
E	0.0347	1.86×10^{-4}

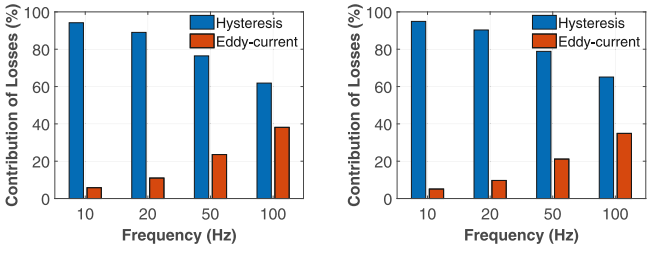

Fig. 12. Contribution of hysteresis and eddy-current losses to the total losses for (a) sample A and (b) sample E at 10 Hz, 20 Hz, 50 Hz, and 100 Hz for stress-free case.

As shown in Fig. 12, at lower frequencies, eddy-current losses are small and hysteresis losses dominate. As the frequency increases, the dominance of the hysteresis losses reduces, while the contribution of the eddy-current losses to the total losses increases. Even though the coefficients of the hysteresis and eddy-current losses could change for the other stress levels, their contribution to the losses should be affected in a similar manner when the frequency increases. In other words, the contribution of eddy-current losses to the total losses compared to the hysteresis losses always increases as the frequency increases since the eddy-current losses grows with the higher order of frequency. Therefore, while the frequency increases, the decrease in the percentage variation of the losses in Figs. 10 and 11 implies that the effect of stress on the eddy-current losses is less compared to the hysteresis losses. Otherwise, we would expect an increase in the percentage variation for the higher frequencies, where the eddy-current losses are more dominant than the lower frequencies. This also aligns with the findings of [35], where M400-50 A grade non-oriented electrical sheets were studied.

Also, it is observed that the percentage variation of the losses is higher for the samples cut along the RD under compressive stress, while it is higher for the samples cut along the TD under tensile stress. This is due to the fact that the material is anisotropic and the impact of the applied stress differs for the RD and TD as discussed in Section 3.1, which also affects the percentage variation of the losses. Similar results were found in [22,23,30,34,35] for different grades of non-oriented electrical steel sheets.

3.5. Combined effect of stress and punching on the iron losses

In Section 3.4, the effect of stress on the iron losses of the punched samples is analyzed thoroughly by considering the percentage variation of the losses from the stress free case of each sample separately. In this section, in order to see how the losses are affected when the effect of stress and punching is combined, the percentage variations of the losses are calculated by taking the loss value of sample A at the stress-free case as a reference for each sample. The loss values of each sample at different stress levels are normalized to the loss value of the sample A at stress-free case. The percentage variation of the losses compared to the reference point is calculated by

$$\Delta p = \frac{p(\sigma) - p_{\mathrm{A}}(0)}{p_{\mathrm{A}}(0)} \tag{11}$$

where $p(\sigma)$ ab $p_{\mathrm{A}}(0)$ are the iron loss density of the sample for the corresponding stress value and iron loss density of the reference sample (sample A) at stress-free case. The calculated percentage variations are given in Figs. 13 and 14 at 1.5 T induction level and different frequencies for the samples cut along the RD and TD, respectively. The x-axis and y-axis show the applied stress values and the number of cutting edges that each sample has, respectively. As the measurement results are at the discrete values, a linear variation was assumed between the measurement points for visualization purposes. The different colors indicate the percentage variation values of the losses, and the iso-value lines connect the regions having the same percentage variation values. It should be noted that (0,0) is the reference point of each sample and the value of the percentage variation is 0.

Figs. 13 and 14 show that, when the combined effect of stress and punching is considered, under compressive stress, the losses increase up to 55.2% and 40.1% for the samples cut along the RD and TD, respectively. The increase in the losses due to the effect of punching increases further with the application of compressive stress. On the other hand, when the applied stress is tensile, at certain levels of the applied stress, the increase in the losses due to the effect of punching is recovered by the applied tensile stress. The value of these required stress levels for the recovery increases as the number of cutting edges increases since the samples become more deteriorated and more tensile stress is required to compensate for this deterioration.

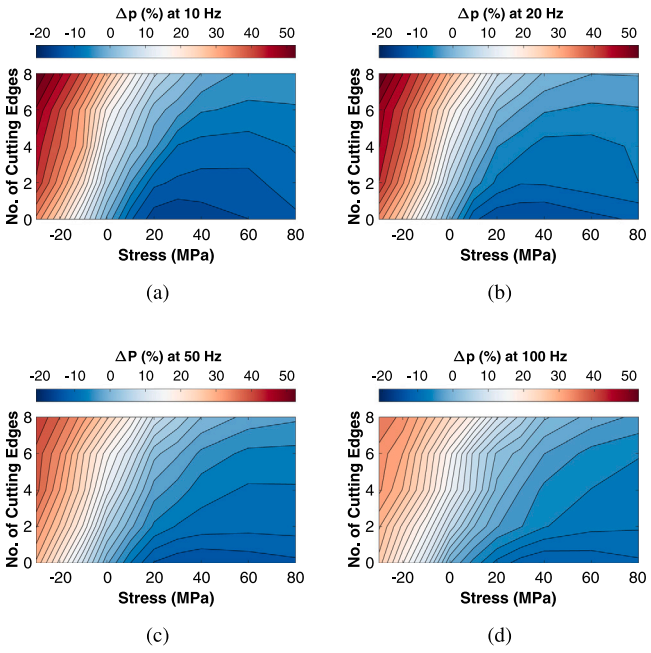

Fig. 13. Percentage variation of the losses (a) at 10 Hz, (b) at 20 Hz, (c) at 50 Hz, and (d) at 100 Hz compared to stress-free case of sample A cut along the RD.

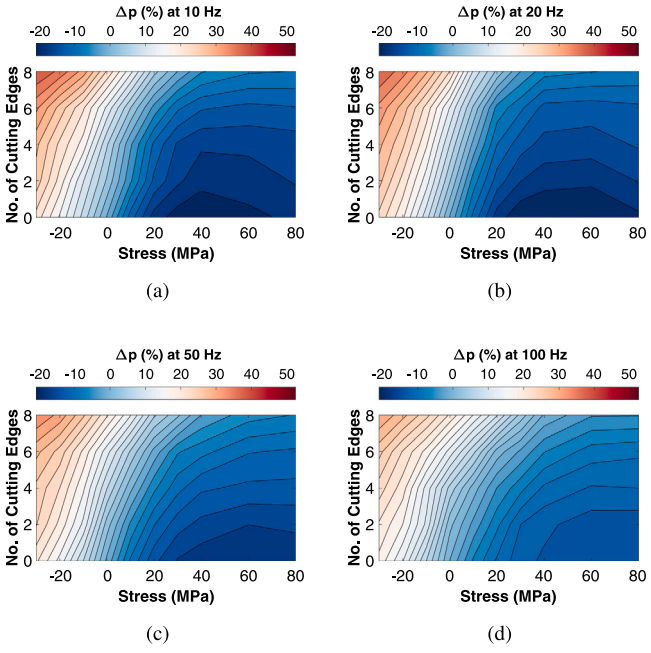

Fig. 14. Percentage variation of the losses (a) at 10 Hz, (b) at 20 Hz, (c) at 50 Hz, and (d) at 100 Hz compared to stress-free case of sample A cut along the TD.

4. Conclusion

The measurement results of the samples cut by punching process and subject to different uniaxial stress levels are presented throughout the paper in detail. The measurement setup and measurement procedure were explained in detail. Afterwards, the results showing the effect of stress on the iron losses of punched samples were analyzed. Lastly, the combined effect of stress and punching on the iron losses were discussed. This is the first study showing the effect of stress on the iron losses of the punched samples and taking the combined effect of stress and punching into account together.

The analyses showed that the effect of stress on the iron losses of the punched samples change depending on the degradation level that the samples have as a result of the cutting process. Within the applied stress range, while the effect of compressive stress on the losses decreases as the number of cutting edges increases, the effect of tensile stress varies with the magnitude of the applied stress. Initially, the applied tensile stress reduces the losses until different thresholds, which increase as the number of cutting edges increases. Then, the losses begin to increase again if the threshold value for the sample is reached. It is observed that these threshold values increase as the deterioration introduced by cutting process increases. Therefore, under high tensile stress, the percentage variation of the losses are higher for the samples having higher number of cutting edges.

It is shown that when the combined effect of stress and punching is considered, the losses introduced by the cutting process can be recovered by certain magnitudes of tensile stress, while the compressive stress further increases the losses introduced by the cutting process. In order to model the magnetic properties and the losses of the electrical sheets used in electrical machines more accurately, the effect of stress and the effect of punching should be combined in the modeling based on the measurements at different magnetization levels.

CRediT authorship contribution statement

I.T. Gürbüz: Conceptualization, Methodology, Software, Validation, Formal Analysis, Investigation, Writing – original draft, Visualization. **F. Martin:** Conceptualization, Software, Writing – review & editing, Visualization. **U. Aydin:** Conceptualization, Writing – review & editing, Visualization. **A.B. Asaf Ali:** Conceptualization, Writing – review & editing. **M. Chamosa:** Conceptualization, Writing – review & editing. **P. Rasilo:** Software, Writing – review & editing. **A. Belahcen:** Conceptualization, Writing – review & editing, Supervision.

Declaration of competing interest

The authors declare that they have no known competing financial interests or personal relationships that could have appeared to influence the work reported in this paper.

References

[1] A. Moses, N. Derebasi, G. Loisos, A. Schoppa, Aspects of the cut-edge effect stress on the power loss and flux density distribution in electrical steel sheets, J. Magn. Magn. Mater. 215 (2000) 690–692.

[2] A. Schoppa, J. Schneider, J.-O. Roth, Influence of the cutting process on the magnetic properties of non-oriented electrical steels, J. Magn. Magn. Mater. 215 (2000) 100–102.

[3] F. Ossart, E. Hug, O. Hubert, C. Buvat, R. Billardon, Effect of punching on electrical steels: Experimental and numerical coupled analysis, IEEE Trans. Magn. 36 (5) (2000) 3137–3140.

[4] D.J.B. Smith, B.C. Mecrow, G.J. Atkinson, A.G. Jack, A.A.A. Mehna, Shear stress concentrations in permanent magnet rotor sleeves, in: Proc. Int. Conf. Electr. Mach., ICEM, Rome, Italy, 2010, pp. 1–6.

[5] A. Borisavljevic, H. Polinder, J.A. Ferreira, On the speed limits of permanent-magnet machines, IEEE Trans. Ind. Electron. 57 (1) (2010) 220–227.

[6] D. Gerada, A. Mebarki, N.L. Brown, K.J. Bradley, C. Gerada, Design aspects of high-speed high-power-density laminated-rotor induction machines, IEEE Trans. Ind. Electron. 58 (9) (2011) 4039–4047.

[7] A. Schoppa, H. Louis, F. Pude, C. Von Rad, Influence of abrasive waterjet cutting on the magnetic properties of non-oriented electrical steels, J. Magn. Magn. Mater. 254 (2003) 370–372.

[8] V. Manescu, G. Paltanea, E. Ferrara, I.V. Nemoianu, F. Fiorillo, H. Gavrila, Influence of mechanical and water-jet cutting on the dynamic magnetic properties of NO Fe-Si steels, J. Magn. Magn. Mater. 499 (2020) 166257.

[9] R. Sundaria, A. Hemeida, A. Arkkio, A. Daem, P. Sergeant, A. Belahcen, Effect of different cutting techniques on magnetic properties of grain oriented steel sheets and axial flux machines, in: Proc. 45th Annu. Conf. IEEE Ind. Electron. Soc, Vol. 1, 2019, pp. 1022–1027.

[10] L. Vandenbossche, S. Jacobs, F. Henrotte, K. Hameyer, Impact of cut edges on magnetization curves and iron losses in e-machines for automotive traction, World Electr. Veh. 4 (3) (2010) 587–596.

[11] N. Boubaker, D. Matt, P. Enrici, F. Nierlich, G. Durand, Measurements of iron loss in PMSM stator cores based on CoFe and SiFe lamination sheets and stemmed from different manufacturing processes, IEEE Trans. Magn. 55 (1) (2019) 1–9.

[12] R. Sundaria, D.G. Nair, A. Lehikoinen, A. Arkkio, A. Belahcen, Effect of laser cutting on core losses in electrical machines—Measurements and modeling, IEEE Trans. Ind. Electron. 67 (9) (2020) 7354–7363.

[13] M. Bali, A. Muetze, Modeling the effect of cutting on the magnetic properties of electrical steel sheets, IEEE Trans. Ind. Electron. 64 (3) (2017) 2547–2556.

[14] S. Elfgen, S. Steentjes, S. Böhmer, D. Franck, K. Hameyer, Continuous local material model for cut edge effects in soft magnetic materials, IEEE Trans. Magn. 52 (5) (2016) 1–4.

[15] G. Loisos, A.J. Moses, Effect of mechanical and nd: YAG laser cutting on magnetic flux distribution near the cut edge of non-oriented steels, J. Mater Process. Technol. 161 (1–2) (2005) 151–155.

[16] M. Bali, A. Muetze, Influences of CO_2 laser, FKL laser, and mechanical cutting on the magnetic properties of electrical steel sheets, IEEE Trans. Ind. Appl. 51 (6) (2015) 4446–4454.

[17] R. Siebert, J. Schneider, E. Beyer, Laser cutting and mechanical cutting of electrical steels and its effect on the magnetic properties, IEEE Trans. Magn. 50 (4) (2014) 1–4.

[18] A. Boglietti, A. Cavagnino, M. Lazzari, M. Pastorelli, Effects of punch process on the magnetic and energetic properties of soft magnetic material, in: Proc. IEEE IEMDC, Cambridge, MA, USA, 2001, pp. 396–399.

[19] Z. Gmyrek, A. Cavagnino, L. Ferraris, Estimation of the magnetic properties of the damaged area resulting from the punching process: Experimental research and FEM modeling, IEEE Trans. Ind. Appl. 49 (5) (2013) 2069–2077.

[20] M. Bali, H. De Gersem, A. Muetze, Finite-element modeling of magnetic material degradation due to punching, IEEE Trans. Magn. 50 (2) (2014) 745–748.

[21] D. Miyagi, N. Maeda, Y. Ozeki, K. Miki, N. Takashi, Estimation of iron loss in motor core with shrink fitting using FEM analysis, IEEE Trans. Magn. 45 (3) (2009) 1704–1707.

[22] D. Miyagi, K. Miki, M. Nakano, N. Takahashi, Influence of compressive stress on magnetic properties of laminated electrical steel sheets, IEEE Trans. Magn. 46 (2) (2010) 318–321.

[23] N. Leuning, S. Steentjes, M. Schulte, W. Bleck, K. Hameyer, Effect of elastic and plastic tensile mechanical loading on the magnetic properties of NGO electrical steel, J. Magn. Magn. Mater. 417 (2016) 42–48.

[24] J. Karthaus, S. Steentjes, N. Leuning, K. Hameyer, Effect of mechanical stress on different iron loss components up to high frequencies and magnetic flux densities, Int. J. Comput. Math. Electr. Electron. (COMPEL) (2017).

[25] O. Perevertov, J. Thielsch, R. Schäfer, Effect of applied tensile stress on the hysteresis curve and magnetic domain structure of grain-oriented transverse Fe-3%Si steel, J. Magn. Magn. Mater..

[26] O. Perevertov, Influence of the applied elastic tensile and compressive stress on the hysteresis curves of Fe-3%Si non-oriented steel, J. Magn. Magn. Mater. 428 (2017) 223–228.

[27] M. LoBue, C. Sasso, V. Basso, F. Fiorillo, G. Bertotti, Power losses and magnetization process in Fe–Si non-oriented steels under tensile and compressive stress, J. Magn. Magn. Mater. 215–216 (2000) 124–126.

[28] Y. Kai, Y. Tsuchida, T. Todaka, M. Enokizono, Influence of stress on vector magnetic property under alternating magnetic flux conditions, IEEE Trans. Magn. 47 (10) (2011) 4344–4347.

[29] Y. Kai, Y. Tsuchida, T. Todaka, M. Enokizono, Influence of stress on vector magnetic property under rotating magnetic flux conditions, IEEE Trans. Magn. 48 (4) (2012) 1421–1424.

[30] A. Baghel, J. Blumenfeld, L. Santandrea, G. Krebs, L. Daniel, Effect of mechanical stress on different core loss components along orthogonal directions in electrical steels, Electr. Eng. 101 (3) (2019) 845–853.

[31] Y. Kai, Y. Tsuchida, T. Todaka, M. Enokizono, Influence of biaxial stress on vector magnetic properties and 2-D magnetostriction of a nonoriented electrical steel sheet under alternating magnetic flux conditions, IEEE Trans. Magn. 50 (4) (2014) 6100204.

[32] O. Hubert, F.S. Mballa-Mballa, S. He, S. Depeyre, Influence of biaxial stress on magnetic behavior of dual-phase steel—Experiments and modeling, IEEE Trans. Magn. 52 (5) (2016) 1–4.

[33] M. Rekik, O. Hubert, L. Daniel, Influence of a multiaxial stress on the reversible and irreversible magnetic behaviour of 3% Si-Fe alloy, Int. J. Appl. Electromagn. Mech. 44 (3–4) (2014) 301–315.

[34] U. Aydin, P. Rasilo, F. Martin, A. Belahcen, L. Daniel, A. Haavisto, A. Arkkio, Effect of multi-axial stress on iron losses of electrical steel sheets, J. Magn. Magn. Mater. 469 (2019) 19–27.

[35] U. Aydin, F. Martin, P. Rasilo, A. Belahcen, A. Haavisto, D. Singh, L. Daniel, A. Arkkio, Rotational single sheet tester for multiaxial magneto-mechanical effects in steel sheets, IEEE Trans. Magn. 55 (3) (2019) 1–10.

[36] K. Yamazaki, H. Mukaiyama, L. Daniel, Effects of multi-axial mechanical stress on loss characteristics of electrical steel sheets and interior permanent magnet machines, IEEE Trans. Magn. 54 (3) (2018) 1–4.

[37] O. Hubert, L. Daniel, R. Billardon, Experimental analysis of the magnetoelastic anisotropy of a non-oriented silicon iron alloy, J. Magn. Magn. Mater. 254 (2003) 352–354.

[38] K. Matsubara, N. Takahashi, K. Fujiwara, T. Nakata, M. Nakano, H. Aoki, Acceleration technique of waveform control for single sheet tester, IEEE Trans. Magn. 31 (6) (1995) 3400–3402.

[39] IEC 60404-2, Magnetic materials – Part 2: Methods of measurement of the magnetic properties of electrical steel strip and sheet by means of an epstein frame, 2008, International Electrotechnical Commission.

[40] S. Zurek, Two-Dimensional Magnetisation Problems in Electrical Steels (Ph.D. thesis), Cardiff University, Whales/United Kingdom, 2005.